Research Square

Preprints are preliminary reports that have not undergone peer review.
They should not be considered conclusive, used to inform clinical practice,
or referenced by the media as validated information.

Investigation and parametric study of the semi-supported steel-composite shear wall at edges under monotonic and cyclic loading

Sina Momeni

sinamomeni936@gmail.com

Institution for Higher Education ACECR Khouzestan

Navid Siahpolo

Institution for Higher Education ACECR Khouzestan

Alireza Jahanpour

Malayer University

Research Article

Keywords: Cyclic Loading, ABAQUS, Semi-Supported Steel Composite Shear wall at the Edges, Bearing Capacity, Nonlinear Analysis

Posted Date: September 2nd, 2026

DOI: https://doi.org/10.21203/rs.3.rs-10624202/v1

License: This work is licensed under a Creative Commons Attribution 4.0 International License.
Read Full License

Additional Declarations: No competing interests reported.

Investigation and parametric study of the semi-supported steel-composite shear wall at edges under monotonic and cyclic loading

Sina Momeni [1], Navid Siahpolo [2*], Alireza Jahanpour [3]

[1] Master of Structural Engineering, Institution for Higher Education ACECR Khouzestan, Iran
sinamomeni936@gmail.com
[2] Assistant Professor, Institution for Higher Education ACECR Khouzestan, Iran
siahpolo@acecr.ac.ir
[3] Assistant Profesor, Malayer University, Iran
a.jahanpour@gmail.com

Abstract

One of the most effective structural systems for resisting lateral loads in buildings is the shear wall. In addition to controlling lateral displacements and resisting horizontal forces, shear walls considerably enhance the overall stiffness of the structure. In this study, semi-supported steel shear walls were investigated, with their strength and ductility improved by applying concrete coatings to the steel plate. The research was conducted in several stages. First, a semi-supported steel shear wall was modeled and analyzed in ETABS to determine the boundary members and identify the critical span. The base model was then converted into a composite semi-supported shear wall. Subsequently, detailed analyses were performed in ABAQUS software under both monotonic and cyclic loading conditions, considering scenarios near and far from the fault. The analyses focused on cyclic behavior, load-bearing capacity, energy dissipation, Von Mises stress distribution, and compressive damage in concrete. The results indicated that applying a concrete coating increased the initial stiffness by approximately 4.5 times and enhanced the ultimate strength by 38%. Moreover, the energy dissipation capacity improved significantly, with increases of 67% and 87% under near-fault and far-fault conditions, respectively. These findings highlight the crucial role of fault proximity in structural behavior. Therefore, designers must give particular attention to the principal structural elements and to the link beam section between the secondary and primary columns when designing such systems.

Keywords: Cyclic Loading, ABAQUS, Semi-Supported Steel Composite Shear wall at the Edges, Bearing Capacity, Nonlinear Analysis

1. Introduction

Shear walls function as large columns that resist seismic forces and are considered essential members in tall reinforced concrete structures, while also serving as efficient lateral load–resisting elements in medium- and low-rise buildings [1]. In terms of failure mechanism, shear walls are capable of sustaining gravity loads even after developing significant cracks, a behavior that cannot typically be expected from conventional columns.Composite steel shear walls represent a modern lateral load–bearing system consisting of a thin steel plate covered with reinforced concrete, connected on one or both sides through shear connectors. In this system, the reinforced concrete cover restrains the steel plate and prevents buckling, thereby enhancing the shear capacity of the wall [2]. The thin steel plate, usually with

* Corresponding Author: siahpolo@acecr.ac.ir

relatively low yield strength, is connected to the boundary elements (beams and columns) by bolts or welding. The behavior of this system resembles that of a plate girder, in which buckling strength can develop in the web plate. To ensure effective performance, the horizontal and vertical boundary elements are designed to remain in the elastic range, which often requires the use of large column sections around the wall. This design approach facilitates the formation of a diagonal tension field and allows utilization of the post-buckling capacity of the steel plate.Extensive studies have been conducted on fully supported composite steel shear walls, but investigations on semi-supported composite steel shear walls remain limited. For instance, Gholhaki et al. (2020) analyzed twelve steel frames with 7, 15, and 30 stories and spans of 5 and 7 bays equipped with SPSWs[1]. Their results indicated that the displacement capacity spectra obtained through energy-based methods were in good agreement with one another. Furthermore, when the roof's center of mass was considered as the target point, the displacement capacity spectrum showed acceptable agreement with the spectrum obtained using the first target case [3]. Similarly, Wang et al. (2019) experimentally examined the seismic behavior of SPSWs and SPCSWs[2]. Their findings revealed that composite shear walls demonstrated superior lateral stiffness, ductility, and energy dissipation capacity compared to conventional SPSWs. However, one drawback of corrugated SPSWs was the "accordion effect," which requires mitigation. Interestingly, this same effect improved the bond between the corrugated steel plate and the concrete, contributing to energy dissipation as a damping mechanism [4]. A more recent development is the SSSW[3], in which the interior plane is considered instead of the full span length [5]. In this configuration, the inner surface does not cover the entire span; rather, the space between two secondary columns within the span is filled with steel plates, concrete, or a combination of both. The secondary columns are welded to the main beams at the top and bottom (commonly through joint connections). The gap between the secondary and primary columns (boundary elements) resembles a link beam, as illustrated in Figure 1.The primary advantages of this wall system include reducing the required cross-section of columns adjacent to the wall, improving the safety of these columns by avoiding complete plasticization, and preventing the formation of floor mechanisms. By contrast, in conventional systems where the wall is directly connected to primary vertical columns, large column cross-sections are required. In such cases, once the column enters the nonlinear range, the overall structural integrity may be compromised due to the formation of plastic hinges [6].

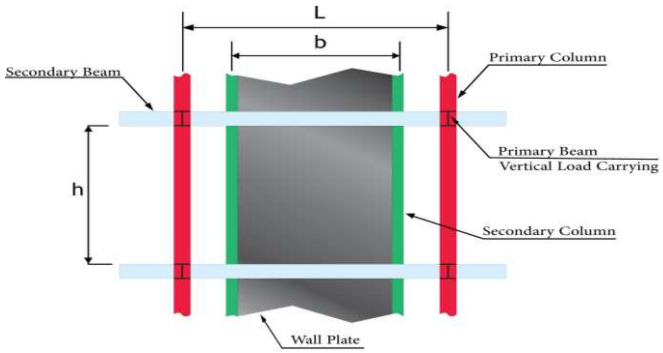


Fig. 1. Schematic details of semi-supported shear wall [7]

Researchers have conducted extensive studies to model concrete using advanced numerical approaches. One such approach, based on the mechanics of continuous media, is the damage model for simulating the behavior of concrete [8]. Previous investigations have demonstrated that combining the damage model with the concrete plasticity model provides a more effective representation of concrete's

[1] Steel plate shear walls
[2] Steel plate reinforced concrete composite shear walls
[3] Semi-supported steel shear wall

nonlinear behavior. The plasticity model for concrete is generally described by isotropic hardening; however, damage is often anisotropic, which must be accounted for in practical applications [9].

In this study, the CDP[1] model was employed to define the damage characteristics of concrete. In general, the application of a periodic load—whether in terms of displacement or force—causing a member to move back and forth is referred to as cyclic loading. The concept of cyclic behavior, or hysteresis, is widely used in earthquake engineering to describe seismic response characteristics such as cyclic energy absorption, stiffness degradation, and strength deterioration in load–deformation cycles. Accordingly, the load–deformation response under reversed loading is expressed as a cyclic or hysteresis curve [10].

In this work, shear wall specimens of both semi-supported steel shear walls (SSSWs) and semi-supported composite steel shear walls (SSCSWs) were subjected to cyclic loading protocols representing near-fault and far-fault conditions, and the results were compared. The composite shear wall model proposed by Zhao and Astaneh-Asl [11], subjected to nonlinear dynamic loading with the cyclic protocol prescribed by the AISC code [12], as well as the initial SSSW model from Jahanpour et al. [13], were validated in ABAQUS software [14] to ensure the reliability of the numerical modeling procedure. Subsequently, an eight-story three-dimensional structure incorporating an SSSW was modeled and designed. In this framework, the concept of an equivalent brace was adopted to simulate the wall plate. The most critical span—defined as the span requiring the largest cross-section of the steel plate and boundary elements—was selected and modeled as the SSSW in ABAQUS. This model was then converted into an SSCSW[2] system following the composite shear wall design provisions of AISC 341-22 [15]. Both models were evaluated under near-fault and far-fault loading protocols, and their cyclic responses were compared. The motivation for introducing this type of shear wall lies in its improved performance in terms of ductility, load capacity, and strength compared with previous shear wall systems. Moreover, given the current trend toward lighter structures, SSCSWs offer an effective alternative to traditional concrete shear walls (CSWs), reducing structural weight while maintaining strength and stability. In this study, the nonlinear behavior of the SSCSW model was examined and compared with that of the SSSW specimen. The parameters investigated included bearing capacity, initial stiffness, ductility, cumulative energy dissipation, Von Mises stress distribution, and compressive damage of the concrete wall. It is important to note that no previous numerical or experimental studies have been carried out on this type of semi-supported wall. The combination of steel and concrete, along with proper reinforcement, was shown to significantly improve seismic behavior by mitigating both partial and global buckling. Accordingly, this paper is the first to propose converting an SSSW into an SSCSW composite system.

2- Methodology Section

2-1- SSSW model details

The semi-supported composite steel shear wall represents a novel lateral load–resisting system. To date, no standard or reference model has been formally developed for this configuration. In previous studies, the small dimensions of the secondary boundary elements in semi-supported steel walls prevented their development into composite steel walls. Consequently, a base model was first designed for this system and analyzed under cyclic loading using ABAQUS software.To construct the base model, the dimensions of the primary and secondary boundary members, along with the thickness of the steel plate, were initially determined using ETABS [16]. The secondary columns and plate thickness were further refined and finalized through Jahanpour and Moharrami's approach [17]. Subsequently, applying the provisions of AISC 341-22, the base wall was converted into a semi-supported composite steel shear wall. Both the steel and composite models were then subjected to cyclic loading analyses. It is important

[1] Concrete damage plasticity
[2] Semi-supported composite steel shear wall

to emphasize the distinction between the behavior of an SSSW and that of a fully constrained shear wall. However, due to the lack of specific design criteria for semi-supported systems, the boundary elements in this study were designed according to the provisions for composite fully constrained shear walls in AISC 341-22. To determine appropriate sections and geometry for the boundary members and the required thickness of the steel plate, an eight-story three-dimensional steel building with a special moment-resisting frame and special concentrically braced frames was modeled in ETABS. In this process, the concept of an equivalent brace was adopted to estimate the initial plate thickness. The building model consisted of 3 spans in the x-direction and 5 spans in the y-direction, each span measuring 5 meters, with a typical story height of 3.2 meters. Model generation, load application, and design checks were conducted according to Iranian Standard 2800 (Fourth Edition) [18] and the Tenth Topic of the National Building Codes [19]. The behavior factor of the SSSW system was selected based on the recommended value for steel shear walls presented in ASCE [20].Based on the calculated stress ratios, the most critical bracing class was identified, and its equivalent was used to determine the plate thickness of the SSSW system. It should be noted that existing standards and codes do not provide a direct equation for converting a brace cross-section to an equivalent plate thickness in SSSW systems. Therefore, the present study applied the equation provided in AISC 341-22 (Equation 1). The authors acknowledge that this equation assumes shear yielding of the steel plate, a mechanism that may not always be realistically expected.

$$t_w = \frac{2A\Omega_s \sin\theta}{l \sin 2\alpha} \quad (1)$$

In Equation 1, α denotes the angle between the slope of the tensile field and the column, which was assumed to be approximately 40°**.** The overstrength factor specified for steel shear walls in AISC 341-22 is 1.2 and was incorporated into the design process. The center-to-center distance between the two secondary columns was taken as 3000 mm. The brace cross sectional area, A, was calculated at the critical span as 4070 mm². The angle θ, representing the inclination between the brace and the column in the bracing system, was assumed to be 45°. Based on these values, the thickness of the steel shear wall plate was determined to be 3 mm. It should be noted that while AISC 341-22 prescribes a minimum wall plate thickness of 10 mm for composite steel shear walls, this requirement does not directly apply to semi-supported systems. Therefore, the same 3 mm thickness was also adopted for the plate in the composite configuration. Figure 2 illustrates the bracing span selected in the ETABS model for converting braces into an equivalent wall plate thickness. As shown, the beams were designed with 2IPE300 sections, the primary columns with BOX 300×25**,** the secondary columns with BOX 250×10**,** and the braces with 2 UPN140. All structural members, except the wall plate, were modeled using ST37 steel**,** while the wall plate was composed of LYP[1] steel with a yield strength of 180 MPa**.**

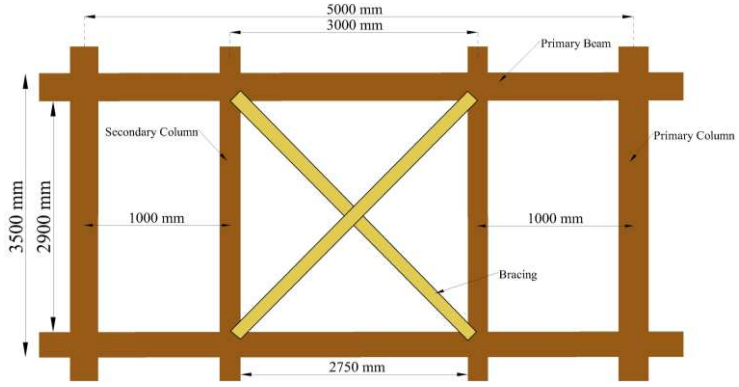


Fig. 2. The critical span to convert the brace to the thickness of the SSSW plate

[1] Low yield point

Since ETABS cannot design the secondary columns and steel plate of the SSSW system, Jahanpour and Moharrami software was used for this purpose. This software is specifically developed to design secondary columns and determine the shear capacity of the SSSW system by considering the thickness of the wall plate. It is based on the formulations and procedures presented in the book by Jahanpour and Moharrami [7]. In this software, several parameters are entered as initial inputs, including the free length of the column, the width of the wall, the thickness of the wall's steel plate, the turning moment, and the estimated shear capacity of the wall. Additional inputs include the type of connection between the secondary columns and boundary beams, the cross-sectional type of the secondary columns, the yield stress of the wall steel plate, the yield stress of the secondary columns, and the values of Bc and Bt, which, according to the program guidelines, influence convergence in the final solution. In ETABS, the section of the secondary columns was modeled as BOX 250×10; however, since the mentioned software does not allow the definition of a box section, this was approximated by replacing the box section with a double channel, using 2 UPN 260 as the initial assumption. Two other inputs, namely the turning moment and the estimated shear capacity, were also entered into the program to calculate the final shear capacity of the wall and check the adequacy of the secondary columns. To determine the turning moment, the shear force applied at each floor was required, which was calculated according to the 2800 standard. The lateral force contribution of the span containing the shear wall was considered at the floor level. For the model designed in this study, the estimated shear capacity (Vs) of the critical span was calculated as 623 kN. The software guidelines state that if, after analysis, the two convergence parameters Pc and Pt are close to 1 and their difference does not exceed 0.005, the final result can be considered valid and the model convergent. According to the program's output (Table 1), Pc and Pt were obtained as 1 and 0.9999, respectively. Therefore, the model converged correctly based on the input parameters, and the BOX 250×10 section for the secondary columns was confirmed to be adequate for the wall steel plate thickness of 3 mm.

Table. 1. Input specifications to Jahanpour and Moharrami software [17]

Specifications	Entrance
Column free length	290 cm
Wall width	300 cm
The thickness of the wall steel plate	3 mm
The amount of turning moment	4795KN.m
The type of connection of secondary-columns with boundary beams	Pinned
Cross-section type of secondary-columns	2UPN 260
The yield stress of the wall steel plate	180 MP
Yield stress of secondary-columns	240 MP
B_c	0.975
B_t	0.975
Estimation of wall shear capacity	623 KN

2-2- Design SSCSW Model

After designing the SSSW model in part 2-1, the wall plate was changed from steel to composite steel by applying concrete on both sides of the steel plate according to the composite shear wall design provisions of AISC 341-22. Since no guideline or standard exists for converting a semi-supported steel shear wall (SSSW) into a semi-supported composite steel shear wall (SSCSW), the criteria for fully supported composite shear walls in AISC 341-22 were adopted to the extent that they did not restrict

the design of the semi-supported system. For example, the vertical and horizontal boundary members, whether steel or composite, were required to satisfy width-to-thickness ratio limits to ensure adequate ductility. Additionally, the strong-column–weak-beam requirement was observed in accordance with the provisions for steel shear wall frames. Clause 6 of AISC 341-22 specifies that a composite shear wall must be designed without a gap between the concrete wall and the boundary members, thereby enhancing the overall stiffness of the system.

After designing the semi-supported steel wall (SSSW) and converting it to a semi-supported composite wall (SSCSW) with concrete on both sides, several variable models were developed. Based on the explanations presented earlier, the variable models and their modifications compared to the base SSSW and expanded SSCSW models are as follows:

- SSCSW OSC model: identical to the developed SSCSW model but with concrete applied to only one side of the steel plate instead of both sides.
- SSCSW CW86 model: identical to the developed SSCSW model but with reduced concrete thickness on each side of the steel plate, from 116 mm in the base model to 86 mm.
- SSCSW PL7 model: identical to the developed SSCSW model but with increased steel plate thickness, from 3 mm in the base model to 7 mm.

Figure 3 illustrates the details of the developed SSCSW model. Following the design and conversion of the SSSW system to the SSCSW configuration, the base and variable models were implemented in ABAQUS and evaluated under the prescribed cyclic loading protocols.

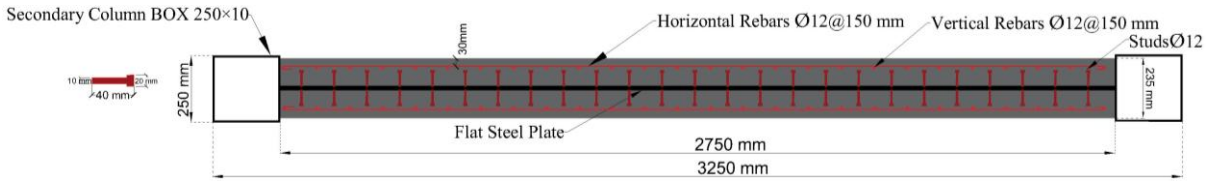


Fig. 3. Section of semi-supported composite steel shear wall

2-3- Numerical modeling process of SSCSW model

A finite element model was developed to investigate the cyclic behavior of the SSCSW system and the interaction between the frame members and the concrete-covered wall plate. The model consisted of a one-story semi-supported composite wall within a single-span frame. In this configuration, the wall plate was supported by secondary columns and connected to upper and lower boundary beams, while the primary columns were welded to the beams. In the software, this connection was represented using a Tie constraint. To connect the concrete wall to the steel plate, studs could have been modeled; however, due to the complex geometry and the excessive analysis time required, a Tie constraint was also applied for this connection. A comparison between monotonic load analyses of the model with Tie constraints and with studs indicated no significant differences in the results. According to the description provided in part 2-1, LYP180 low-strength steel was used for the wall plate, while ST37 steel was adopted for the remaining members. Figure 4(A) illustrates the semi-supported SSCSW model, and Figure 4(B) presents the stress–strain curves of the steels. In this study, a damage model was defined for both steel and concrete; therefore, only the stress and strain values corresponding to the fracture region were included in the stress–strain curves, and the initial linear portion of the diagram was omitted.

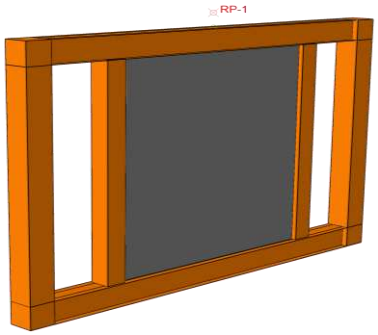


Figure. 4. A.

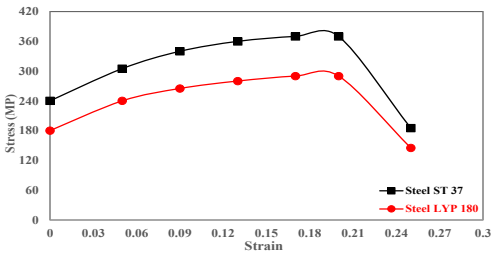


Figure. 4. B.

Fig. 4. SSCSW numerical model and steel stress-strain cure; (A): Developed SSCSW model in ABAQUS and (B): Stress-strain curve of ST37 and LYP180 steel

In order for the finite element model to accurately reproduce the experimental behavior and capture cyclic strength deterioration, a damage model was defined in the software for the materials used. For concrete, the concrete damaged plasticity (CDP) model was adopted to represent the damage behavior under both tension and compression. In this study, the Hognestad equation [21] was employed to describe the compressive damage behavior of concrete, as presented below:

$$\sigma_c = f_c''\left(\left(\frac{2\varepsilon_c}{\varepsilon_0}\right) - \left(\frac{\varepsilon_c}{\varepsilon_0}\right)^2\right) \quad (2)$$

In equation (2), σ_c is the maximum compressive stress of concrete, ε_c is the strain values, f_c'' is the compressive strength of concrete, which is obtained from equation (3):

$$f_c^{''} = f_c^{'} K_s \quad (3)$$

In equation (3), K_s is a coefficient whose value differs for concretes with different compressive strength. In this work, considering the use of concrete with a compressive strength of 25 MPa, its value is 0.95. Also, in equation (2) ε_0, the strain is like the maximum stress and its value is calculated from equation (4):

$$\varepsilon_0 = 18\frac{f_c''}{E_0} \quad (4)$$

In equation (4), E_0 is the initial elasticity modulus of concrete. To calculate the stress-strain curve of concrete in tension, considering that the models this paper are numerical and the experimental results of cylinder splitting or direct tension tests are not available, to obtain the maximum tensile stress, we can use the equation (5) used [22].

$$\sigma_t = 0.3f_c''^{\frac{2}{3}} \quad (5)$$

In equation (5), σ_t is the maximum tensile stress. The concrete stress-strain curve is obtained by calculating and placing in the mentioned equations (Figure. 5).

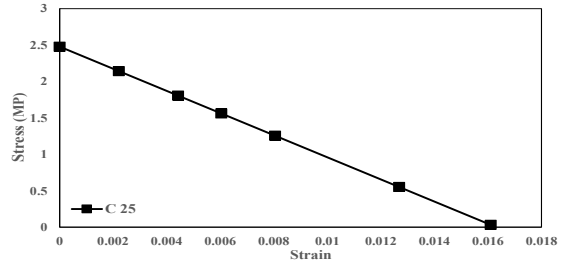


Fig. 5. A.

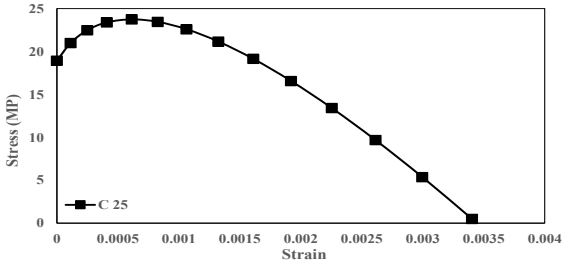


Fig. 5. B.

Fig 5. Behavioral model of concrete with 25 MPa strength in compression and tension; (A):The behavior of concrete in the tensile zone with a strength of 25 MPa. (B): The behavior of concrete in the compression zone with a strength of 25 MPa

The steel damage model was defined as ductile damage in order to capture the localized deterioration of steel elements and to reflect strength degradation in the numerical outputs so that the results closely matched experimental observations. In ABAQUS, the ductile damage behavior is characterized through specific input parameters. Three key strain-related parameters were considered, corresponding to ultimate stress, triaxial stress, and strain rate. The triaxial stress parameter was calculated using the following equation:

$$\eta = \frac{-\frac{1}{3}(\sigma_{xx}+\sigma_{yy}+\sigma_{zz})}{\sigma_{mises}} \quad (6)$$

In equation (6), η is the 3-axis stress, $\sigma_{xx}.\sigma_{yy}.\sigma_{zz}$ is respectively the stress tensor in x, y, and z direction, and σ_{mises} is Von Mises stress. In the software, the ductile damage model is used in terms of energy failure for steel elements in such a way that the energy failure according to the dimensions of each component and according to the type of steel and the corresponding stress−strain curve (Figure 4−B), using the equation (7) is calculated:

$$G_f = \int_{\bar{\varepsilon}_0^{pl}}^{\bar{\varepsilon}_f^{pl}} L\,\sigma_y\, d\bar{\varepsilon}^{pl} \quad (7)$$

In equation (7), G_f fracture energy, $\bar{\varepsilon}_0^{pl}$ is the strain corresponding to the beginning of fracture, which is the strain corresponding to the ultimate stress, $\bar{\varepsilon}_f^{pl}$ is the strain corresponding to the end of the fracture stress, σ_y is the ultimate stress according to the type of steel used for each element and L for 2D elements are equal to the length of each component (beam, column, etc.) and for 3D elements, it is calculated from the following equation:

$$L = l.\,b.\,h \diagup \text{The area of the largest 2D surface of the element} \quad (8)$$

In equation (8), L is the average element length for 3D elements, l is the element length, b is the element width, and h is the element length in the z-direction. According to the above explanations, failure of the type of failure energy is defined according to equation (7) for each member according to (Table 2):

Table 2. Fracture energy for elements in SSCSW and SSSW models

Parameter / Section	Failure energy(G_f)
Primary column	6475
Secondary-column	4625
Beam	5550
Plate wall	50875

After modeling and determining the materials and boundary conditions, the loading protocol is defined. In this article, the far and near fault loading protocol SAC [23] is used to check the behavior of the models. The software defines the two protocols according to (Figure 6). Are.

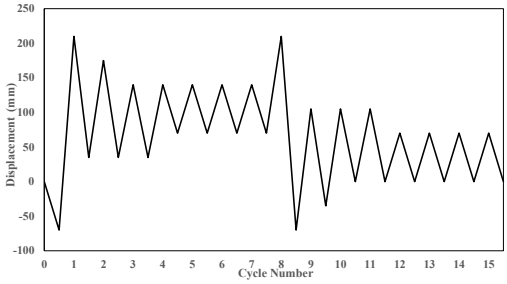


Fig. 6. A.

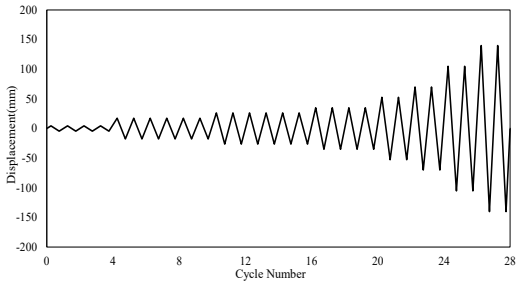


Fig. 6. B.

Fig. 6. SAC far and near fault loading protocol; (A): SAC near-fault loading protocol generalized to the models studied in this paper and (B): SAC far-fault loading protocol is generalized to the models studied in this paper

3- Validation

3-1- Validation of the SSSW model by Jahanpour et al

For validation, this study employed model number 1 from Jahanpour et al. and model number 1 from Zhao and Astaneh-Asl. The validation process was carried out using ABAQUS software. The specimens were modeled using a combination of shell elements and three-dimensional solid elements. The reliability of the investigated parameters depends on the accuracy of the analytical results. To ensure this, experimental data from SSSW and SSCSW models were utilized as benchmarks. An analytical model was first constructed based on the conditions and specifications of an available experimental model, and the analytical and experimental results were compared. However, since no prior research exists for the SSCSW model, the validation of the composite portion was performed using data from a fully supported composite shear wall. When the analytical results demonstrated acceptable agreement with the experimental findings, it was concluded that the modeling approach and

assumptions applied in the analysis were sufficiently accurate, making the model reliable for investigating different parameters. Figure 7 presents the details of the experimental model developed by Jahanpour et al.



Fig. 7. Experimentally model of semi-supported steel shear wall along with the introduction of wall members[13]

In the validation model of Jahanpour et al., two different types of steel were used in the SSW specimen: the wall plate was made of ASTM A36 steel, while the frame members were fabricated from plates conforming to ASTM A572. Since the original study was experimental and the current validation is numerical, the yield and ultimate stress–strain values had to be converted from engineering values to true values. For this purpose, after constructing the model in ABAQUS, a standard tensile test was simulated, and the stress–strain data were extracted. In the numerical model, the ultimate stress for the wall plate was 145 MPa, while for the other members it was 245 MPa. The thickness of the wall plate in the validation model was 1 mm. The primary columns outside the plate had an RHS120×80×4 section, the secondary columns were IPE100, and the beams were IPE120.In ABAQUS, two plastic hardening rules can be defined for materials: isotropic hardening, in which the yield surface expands with plastic strain, and kinematic hardening, in which the yield surface translates without expansion. For cyclic analyses, the kinematic rule or a combination of isotropic and kinematic hardening is generally preferred, with the combined rule being the most accurate since it incorporates the advantages of both and compensates for their individual limitations. All structural members were modeled using S4R four-node shell elements with reduced integration. Each node included six degrees of freedom: three translational (Ux, Uy, Uz) and three rotational (θx, θy, θz). The S4R element accounts for large rotations and strains, as well as thickness variations, making it suitable for analyses involving significant deformation, materials with non-zero effective Poisson's ratio, and cases where geometric nonlinearity occurs. The loading protocol applied to this model was cyclic loading under far-fault conditions, expressed in terms of drift cycles, and followed the ECCS 1986 standard [24]. The load was applied to a reference point (RP) defined in the numerical model. The shear wall was connected to this reference point through a coupling constraint, and the force–drift response at the node was recorded for comparison with the experimental results. Figure 8 illustrates the cyclic loading protocol under far-fault conditions for the first model in the study of Jahanpour et al., together with the finite element model developed in ABAQUS.

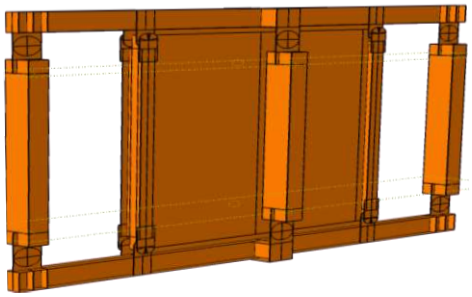


Fig. 8. A.

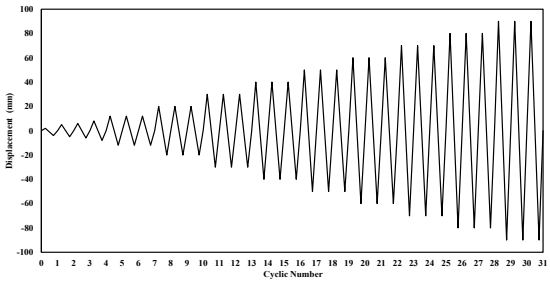


Fig. 8. B.

Fig. 8. Far-fault cycle loading protocol Eccs1986 extended to Jahanpour et al. model and finite element model; (A):The finite element model of the experimental sample in ABAQUS (B):Far-fault cycle loading protocol Eccs1986 [24]

Figure 9 compares the cyclic response of the numerical model with the experimental results. The findings indicated that the initial stiffness of the numerical model was significantly higher than that of the experimental model. In the experimental specimen, the initial stiffness was approximately 2 kN/mm, while in the numerical model it reached about 5 kN/mm, representing a difference of roughly 150%. This discrepancy in stiffness, which corresponds to the slope of the initial tangent of the cyclic curve, gradually decreased once the response entered the nonlinear range, where closer agreement was observed. However, the difference remained noticeable during the early loading stages and in large displacement cycles. The lower stiffness observed in the experimental model is primarily attributed to the slip of the studs connecting the wall plate to the boundary angles. These slips also caused tearing in the wall plate during the test, which resulted in horizontal relative displacements between the plate and the angles, thereby reducing the overall stiffness. In contrast, in the finite element model, the Tie constraint was used to idealize the connection, effectively preventing slip and eliminating relative horizontal movement between the plate and the angles. At later stages of loading, when the tension field was well established in the wall plate and stress transfer between the plate and the boundary angles dominated the behavior, the effect of slip diminished compared to the initial stages. Consequently, the differences between the two models became less pronounced. With increasing applied load according to the loading protocol, the bearing capacities of the numerical and experimental specimens converged, and their ultimate strengths showed only a small discrepancy. The ultimate strength of the experimental model was approximately 69 kN, while that of the numerical model was about 79 kN, reflecting a difference of nearly 10%.

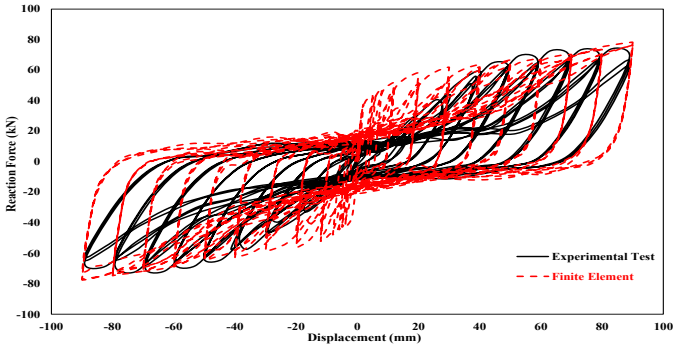


Fig. 9. Comparison of the cyclic output of validation of the present article with the experimental sample of model number 1 of Jahanpour et al. article [13]

3-2- Validation of Zhao and Astaneh-asl's CSW model

Following the validation of the SSSW model, an additional validation was conducted to account for the composite steel shear wall considered in this study. For this purpose, Model 1 from the work of Zhao and Astaneh-asl was selected. The experimental configuration consisted of a two-story shear wall within a two-span frame, where the wall steel plate was connected to the surrounding beams and columns using bolted connections, resulting in a fully symmetrical system. In this setup, the beams were attached to the frame columns, and the shear wall was fastened to the boundary members by bolts. A layer of concrete was placed on one side of the wall and anchored to the steel plate using bolts to prevent slipping of the concrete surface under lateral loading. Longitudinal and transverse rebars were embedded within the concrete core. The boundary columns were fixed at their bases, while gusset plates at the top and bottom of the boundary columns were welded. In the numerical model developed by Zhao and Astaneh-asl, shell elements were used to represent the steel members, and three-dimensional solid elements were applied to the concrete wall to properly account for the embedded reinforcement. The wall steel plate material was ASTM A36, while the frame members were made of plates specified according to ASTM A572. The definition of material and geometric properties—including integration technique, boundary conditions, support conditions, and meshing—was consistent with the procedures outlined in Section 3-1. Figure 10 presents the finite element model of the shear wall and its surrounding frame, together with the cyclic loading protocol applied in this validation.



Fig. 10. A.

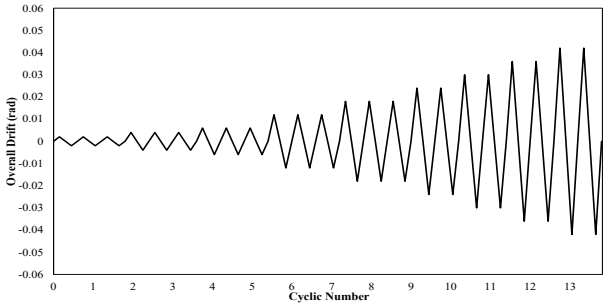


Fig. 10. B.

Fig. 10. AISC far-fault cycle loading protocol extended to Zhao and Astaneh-asl model and finite element model;(A):Finite element model of experimental sample in ABAQUS (B):AISC far-fault cycle loading protocol [12]

The numerical validation results demonstrated that the initial stiffness obtained from the cyclic response of the finite element model was reasonably close to that of the experimental specimen. In the experimental sample, the initial stiffness was measured at 171 kN/mm, while in the numerical model it was 204 kN/mm, indicating a difference of approximately 19%. With increasing load during cyclic analysis, the experimental specimen exhibited slightly higher strength compared to the numerical model, resulting in an ultimate strength of 2780 kN for the experimental sample and about 2700 kN for the numerical model. This difference of roughly 3% confirms that the two responses are in good agreement. The small discrepancy in ultimate strength is mainly attributed to the more pronounced pinching effect observed in the cyclic response of the experimental sample. This effect can be explained by the slip of the bolts connecting the wall plate to the boundary members and the associated local damage to the steel plate during testing. In contrast, in the numerical model, bolts and studs were not modeled explicitly due to the complexity of geometry and the significant computational cost. Instead, Tie constraints were employed, which eliminated slip between the wall plate and boundary members, thereby reducing pinching compared to the experimental response. These differences led to minor variations in horizontal displacements and stiffness degradation between the two models. Overall, the validation process confirms that the numerical model provides sufficiently accurate results compared to the experimental data, and the adopted modeling approach is reliable for investigating the behavior of SSCSW systems in this study. Figure 11(A) illustrates the validation results under monotonic loading, while Figure 11(B) presents the comparison under cyclic loading far from the fault.

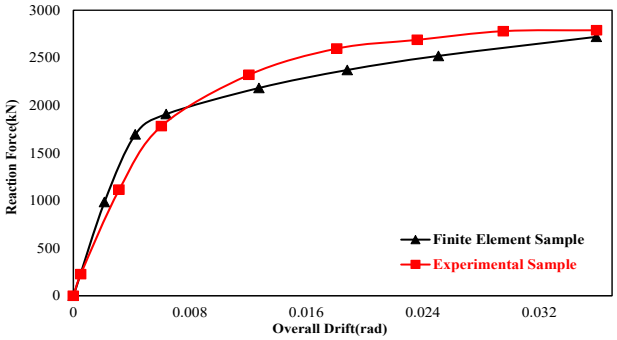


Fig. 11. A.

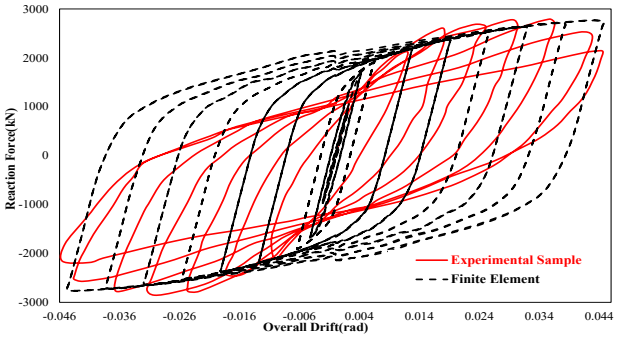


Fig. 11. B.

Fig. 11. Comparison of numerical and experimental validation samples of model 1 article Zhao and Astaneh-asl;(A):Comparison of numerical and experimental output under monotonic loading (B):Comparison of numerical output and experimental sample under cyclic loading[11]

4- Results

4-1- Behavior output of SSSW model and SSCSW models under monotonic loading

After designing the base SSSW model, developing it into the SSCSW sample, and validating the numerical models against the experimental studies of Jahanpour et al. and Zhao and Astaneh-asl, the next step was to compare the performance outputs of the two systems together with the variable models defined in Section 2-2. The models designed and analyzed in this study were subjected to both monotonic loading and cyclic loading protocols representative of near-fault and far-fault SAC records. The key results examined included hysteresis behavior, pushover capacity, ductility, energy dissipation, initial stiffness, ultimate strength, Von Mises stress distribution in the SSSW model, and compressive damage distribution in the SSCSW models. The primary objective was to evaluate the improvements provided by the SSCSW system relative to the SSSW. Under monotonic loading, the models were pushed to a lateral displacement corresponding to 4% of the total frame height. The results indicated that the SSCSW, with concrete layers applied to both sides of the steel plate, exhibited higher initial stiffness, greater ductility, and significantly improved ultimate strength. The increase in ultimate strength was approximately 35% compared to the SSSW. This finding highlights the effectiveness of the concrete cover in enhancing structural capacity. It was also observed that in the SSCSW model, as the applied load increased, the elastic slope of the response improved until the concrete cover began to crack. Once the maximum system capacity was reached—around 3200 kN—the concrete cover near the beam-column connections experienced crushing. This damage led to a reduction in both stiffness and ultimate load capacity, as evidenced by the slightly descending slope in the nonlinear region of the SSCSW response. Similar trends were observed in the variable composite models. These findings suggest that using a concrete cover, especially when a gap is provided between beams and columns to reduce stress concentrations, can substantially improve the performance of semi-supported shear walls. Figure 12 illustrates these behavioral differences.

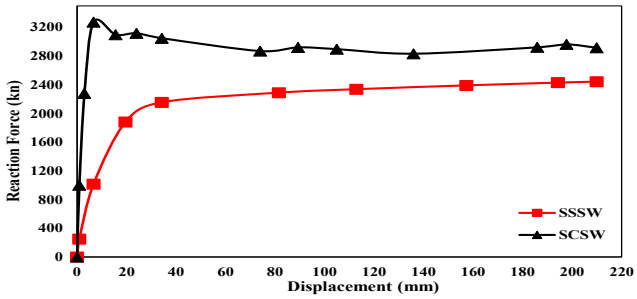


Fig. 12. Comparison of the capacity curve obtained from monotonic load analysis for SSSW and SSCSW models

After designing the base SSSW model, developing it into the SSCSW sample, and validating the numerical models against the experimental studies of Jahanpour et al. and Zhao and Astaneh-asl, the next step was to compare the performance outputs of the two systems together with the variable models defined in Section 2-2. The models designed and analyzed in this study were subjected to both monotonic loading and cyclic loading protocols representative of near-fault and far-fault SAC records. The key results examined included hysteresis behavior, pushover capacity, ductility, energy dissipation, initial stiffness, ultimate strength, Von Mises stress distribution in the SSSW model, and compressive damage distribution in the SSCSW models.The primary objective was to evaluate the improvements provided by the SSCSW system relative to the SSSW. Under monotonic loading, the models were pushed to a lateral displacement corresponding to 4% of the total frame height. The results indicated that the SSCSW, with concrete layers applied to both sides of the steel plate, exhibited higher initial stiffness, greater ductility, and significantly improved ultimate strength. The increase in ultimate strength was approximately 35% compared to the SSSW. This finding highlights the effectiveness of the concrete cover in enhancing structural capacity. It was also observed that in the SSCSW model, as the applied load increased, the elastic slope of the response improved until the concrete cover began to crack. Once the maximum system capacity was reached—around 3200 kN—the concrete cover near the beam-column connections experienced crushing. This damage led to a reduction in both stiffness and ultimate load capacity, as evidenced by the slightly descending slope in the nonlinear region of the SSCSW response. Similar trends were observed in the variable composite models. These findings suggest that using a concrete cover, especially when a gap is provided between beams and columns to reduce stress concentrations, can substantially improve the performance of semi-supported shear walls. Figure 12 illustrates these behavioral differences.

In the variable models SSCSW-OSC and SSCSW-CW86, a reduction in ultimate strength was observed compared to the reference SSCSW model. However, a noteworthy finding was that these two variable models exhibited almost identical behavior. Specifically, the SSCSW-CW86 model (with a reduced concrete cover thickness of 86 mm on each side of the steel plate) and the SSCSW-OSC model (with a concrete cover on only one side of the steel plate) demonstrated similar initial stiffness and ultimate strength values. The ultimate load capacity for both variable models was approximately 2795 kN, while the corresponding value for the reference SSCSW model was 2964 kN. Overall, the ultimate strength under monotonic loading in these two variable models decreased by about 6% relative to the SSCSW specimen. In contrast, the SSCSW-PL7 variable model, which featured an increased steel plate thickness from 3 mm to 7 mm compared to the SSCSW model, showed a significant enhancement in both initial stiffness and ultimate load-carrying capacity. The ultimate strength of this model was estimated to be 4023 kN, representing an approximate 36% increase compared to the reference SSCSW model. Figure 13 illustrates the monotonic load–displacement performance of the variable models in

comparison with the developed SSCSW specimen, clearly highlighting the influence of geometric and material modifications on the structural behavior.

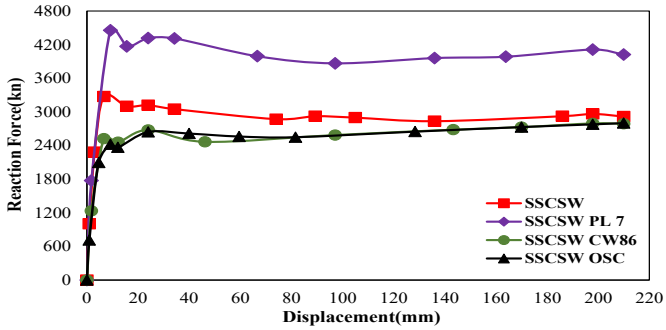


Fig. 13. Comparison of the capacity curve obtained from monotonic loading analysis for variable models compared to the SSCSW sample

4-2- Behavior output of SSSW model and SSCSW models under cyclic loading

After evaluating the base and variable models under monotonic loading in Section 4-1, the same models were subjected to cyclic loading near and far from the fault using the SAC loading protocol described in Section 2-3. The results of the base SSSW and the developed SSCSW models were first compared under these two protocols, as illustrated in Figure 14. The analyses showed that the initial stiffness of the SSCSW model was 469 kN/mm, while in the SSSW model it was only 104 kN/mm. This represents an approximately 350% increase in initial stiffness, attributed to the presence of concrete layers on both sides of the steel plate in the SSCSW configuration. The ductility factor obtained under the far-fault loading protocol was 25 for the SSCSW model compared to 10 for the SSSW model, indicating a 150% increase in ductility due to the addition of concrete. Similar results were observed under the near-fault loading protocol, confirming that the improvement in ductility is consistent across different loading patterns and is not dependent on the specific protocol applied. In terms of ultimate strength, the SSCSW model reached 3004 kN, while the SSSW model reached 2353 kN, reflecting a 28% increase in ultimate strength. This improvement, however, is slightly lower than the 35% increase observed under monotonic loading. It is important to note that plate tearing was not considered in the developed numerical models. Therefore, the reported values represent an idealized case in which failure

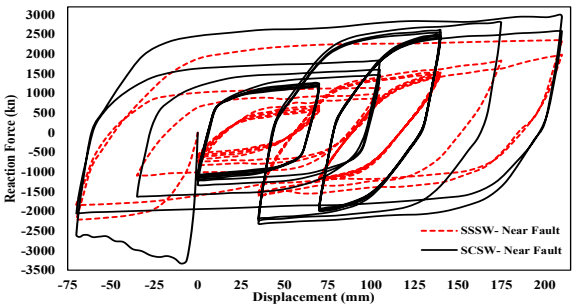


Fig. 14. A.

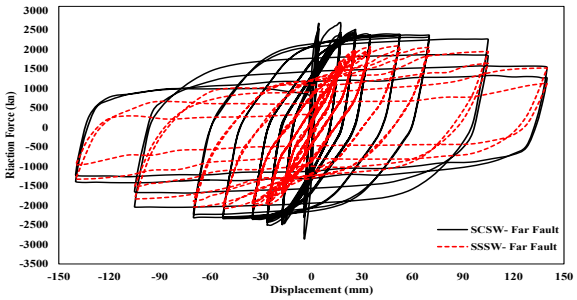


Fig. 14. B.

Fig. 14. Cyclic curve for SSSW and SSCSW model; (A):SSSW and SSCSW model under near-fault pattern (B): SSSW and SSCSW model under far-fault pattern

The variable models were then subjected to cyclic loading near the fault, and their results were compared with those of the developed SSCSW model. For the SSCSW CW86 model, the initial stiffness was 360 kN/mm, representing a 30% reduction compared to the SSCSW sample (469 kN/mm). The ultimate strength of the SSCSW CW86 model was 2915 kN, only 3% lower than that of the SSCSW model (3004 kN) (Figure 15.A). This indicates that once the concrete cover is damaged during the initial cycles, a considerable portion of its strength is lost, and the system behavior becomes similar to that of a purely steel wall, which explains the close ultimate strengths of the two models. For the SSCSW OSC model, the initial stiffness was 346 kN/mm, showing a 36% decrease compared to the SSCSW model. The ultimate strength of the SSCSW OSC model was 2806 kN, corresponding to a 7% reduction relative to the SSCSW model (Figure 15.B). In contrast, the SSCSW PL7 model exhibited a significant improvement in performance. Its initial stiffness was 636 kN/mm, which is 35% higher than that of the SSCSW model. Moreover, the ultimate strength reached 4042 kN, representing a 34% increase compared to the SSCSW model (Figure 15.C).

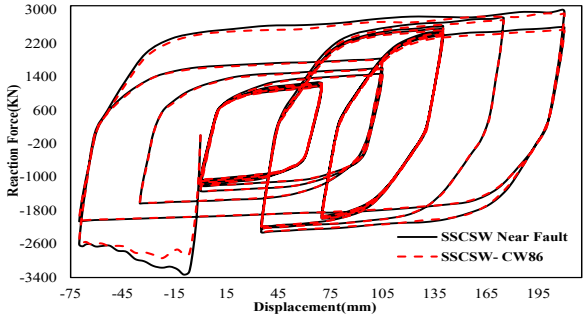


Fig. 15. A.

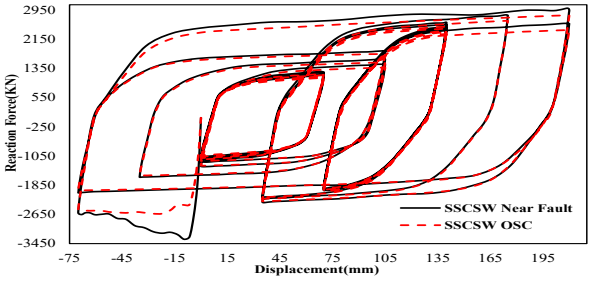


Fig. 15. B.

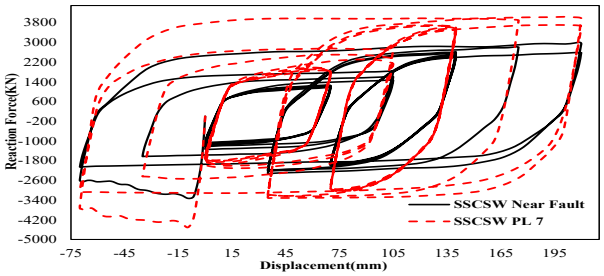


Fig. 15. C.

Fig. 15. Comparison of variable models with the developed SSCSW model under near-fault loading; (A):SSCSW and SSCSW CW86 model under near-fault pattern (B):SSCSW and SSCSW OSC model under near-fault pattern (C):SSCSW and SSCSW PL 7 model under near-fault pattern

4-3- Comparison of energy dissipation in the SSSW model and SSCSW models

Following the cyclic loading analysis in part 4-2, the cumulative energy dissipation of the models was evaluated under both near-fault and far-fault loading conditions. Under the far-fault protocol, the cumulative energy dissipation of the SSSW model was 3.3 MJ, whereas the SSCSW model reached 5.5 MJ, corresponding to a 67% increase in the composite wall (Figure 16.A). Under the near-fault protocol, the cumulative energy dissipation of the SSCSW model was 4.84 MJ compared to 2.8 MJ for the SSSW model, representing a 73% increase in the composite wall (Figure 16.B).

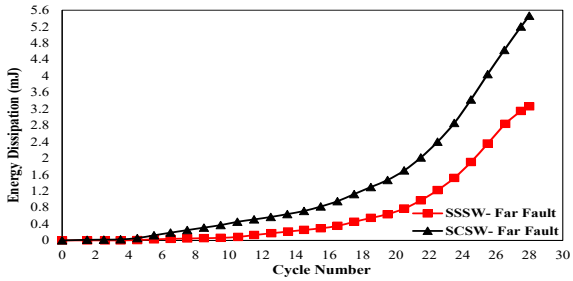


Fig. 16. A.

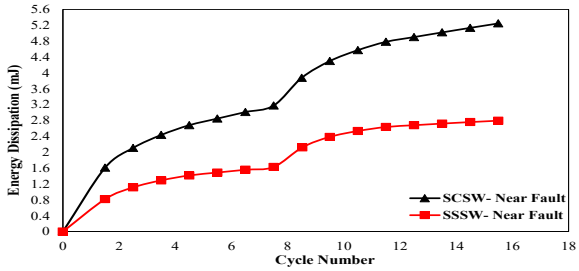


Fig. 16. B.

Fig. 16. Comparison of cumulative energy dissipation in SSSW and SSCSW models under loading near and far from the fault; (A):The amount of energy dissipation of each cycle in the pattern away far-fault for the SSSW and SSCSW models (B):The amount of energy dissipation of each cycle in the pattern away near-fault for the SSSW and SSCSW models

After examining the two samples above, the energy dissipation of the variable models was compared with the SSCSW sample under the near-fault pattern. First, the results of the SSCSW CW86 model were compared with SSCSW. The results showed that in the SSCSW CW86 sample, the maximum amount of cyclic energy dissipation was calculated as 4.6 MJ, and according to the amount of cyclic energy dissipation of 4.84 MJ in the SSCSW sample, it shows a decrease of 5% (Figure 17. A). The comparison of energy dissipation in the SSCSW OSC sample compared to the SSCSW sample showed that the amount of energy dissipation in both models was 4.4 MJ, and reducing the concrete cover on

the steel plate of the wall does not affect the cumulative energy dissipation (Figure 17. B). The comparison of the cumulative energy dissipation in the SSCSW PL 7 model with the SSCSW sample showed that the highest cyclic cumulative energy dissipation in the SSCSW PL 7 model is 7.2 MJ, which shows a significant increase of 49% in the cumulative energy dissipation compared to the SSCSW sample. (Figure 17. C).

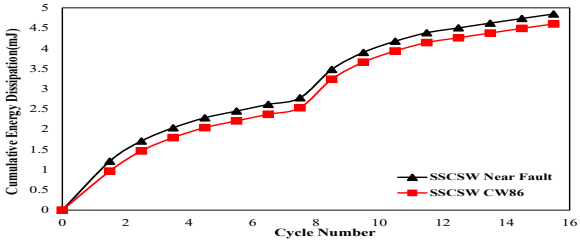


Fig. 17. A.

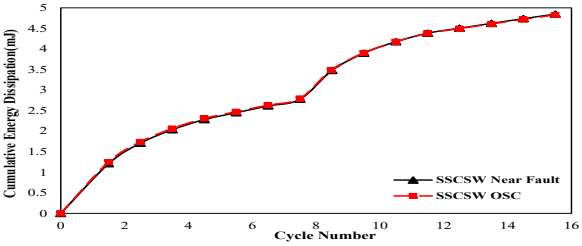


Fig. 17. B.

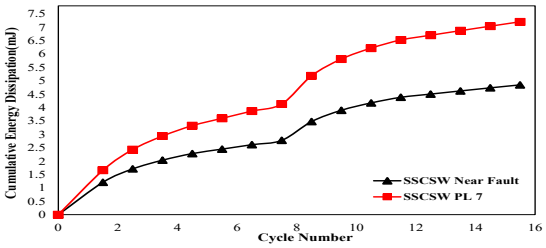


Fig. 17. C.

Fig. 17. Comparison of the cumulative energy dissipation of variable models with the developed model SSCSW under near-fault loading; (A):Comparison of the cumulative energy dissipation of two SSCSW and SSCSW CW86 models under the near-fault pattern (B):Comparison of the cumulative energy dissipation of two SSCSW and SSCSW OSC models under the near-fault pattern (C):Comparison of the cumulative energy dissipation of two SSCSW and SSCSW PL 7 models under the near-fault pattern

5- Von Mises stress distribution and examination of damage to the concrete wall

Figure 18 presents the Von Mises stress distribution of the SSSW model under near- and far-fault loading, as well as the compressive damage distribution in the concrete wall of the SSCSW model for the same SAC protocols. In Figure 18.A, under the near-fault pattern, the maximum displacement occurs during the first cycle, and the highest stress concentration appears at the beam-to-primary column connection. This region reaches the collapse zone with a peak stress of 253 MPa. In Figure 18.B, representing the far-fault protocol in the final cycles, both the beam-to-primary column connections and the beam-to-secondary column joints enter the collapse zone, with the maximum stress reaching 256 MPa. These results confirm that, under far-fault loading, the structural response remains consistent with the expected wall behavior, preventing severe damage to the main frame elements. The contribution of the concrete cover plays a crucial role in this performance. Specifically, under far-fault loading, damage initiates gradually from the fourth cycle and progresses until the tenth cycle, at which point the concrete wall is completely crushed. In contrast, under near-fault loading, the concrete cover undergoes abrupt failure during the initial cycles, with approximately 60% of the cover crushed in the

first cycle (Figures 18.C and 18.D). This sudden degradation transfers additional forces to the frame-wall system, pushing the primary structural elements, particularly the columns, into nonlinear behavior. Consequently, it is recommended that designers carefully consider the performance of primary frame columns under near-fault protocols. Furthermore, since the portion of the beam located between the secondary and primary columns behaves similarly to a link beam, its nonlinear response should be specifically evaluated in future studies.

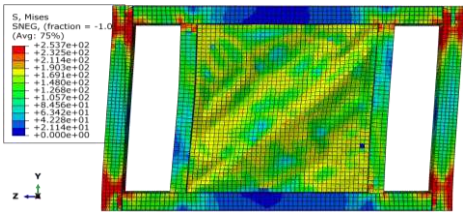


Fig. 18. A.

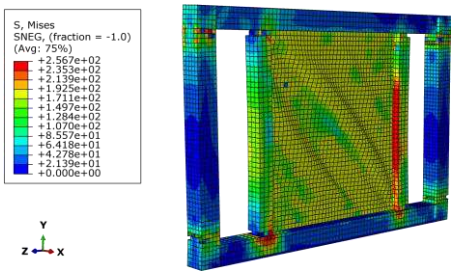


Fig. 18. B.

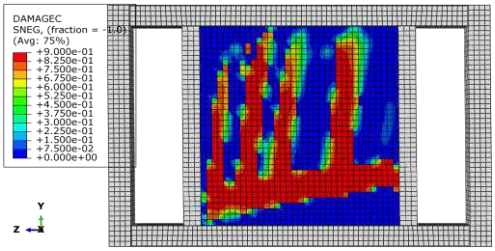


Fig. 18. C.

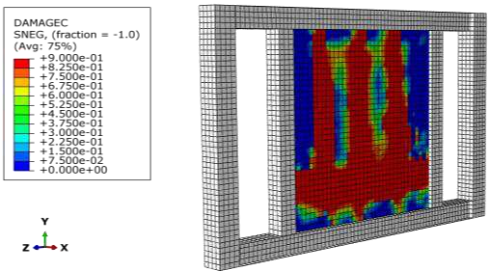


Fig. 18. D.

Fig. 18. Von Mises stress distribution in the SSSW model and compression damage distribution in the concrete wall for the SSCSW model, under loading near and far from the fault; (A): Von Mises stress distribution in the SSSW model under the near-fault model (B): Von Mises stress distribution in the SSSW model under the far-fault model (C):Compressive damage distribution of SSCSW model concrete under the near-fault model (D):Compressive damage distribution of SSCSW model concrete under the far-fault model

5-1- Von Mises stress distribution in the panel zone in the developed SSCSW model

Following the investigation of the models under monotonic and cyclic loading near and far from the fault using the SAC protocol, the performance of the beam located between the primary and secondary columns in the SSCSW sample was analyzed. Figure 19 illustrates the maximum Von Mises stress

distribution within the panel zone of the SSCSW model. The results indicate that the peak Von Mises stress developed at the connection between the secondary column and the top beam on the left side of the frame, reaching a value of 257 MPa. This maximum stress corresponds to regions where element removal had not yet occurred. However, part of the connection between the secondary column and the beam experienced element removal. Based on the adopted ductile damage model for steel, once the local stress exceeded the predefined ultimate stress of 370 MPa, element deletion was triggered at the specified location, confirming the occurrence of localized failure.

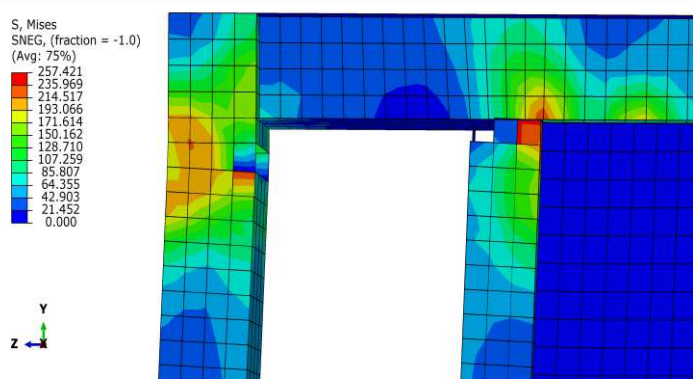


Fig. 19. The maximum Von Mises stress distribution (MPa) in the panel zone and the beam between the primary column and the left secondary column in the upper beam in the SSCSW sample

6- Conclusion

This study investigated the cyclic and monotonic behavior of semi-supported steel shear walls (SSSW) and semi-supported composite steel shear walls (SSCSW) through finite element modeling and validation against experimental benchmarks. The following conclusions can be drawn:

1. Converting SSSW to SSCSW by adding concrete cover on both sides of the steel plate significantly enhanced performance. Initial stiffness increased by approximately 350%, ductility improved by a factor of 2.5, and ultimate strength rose by 28–35% depending on the loading protocol.

2. Energy dissipation capacity of the SSCSW model increased markedly compared to SSSW, with improvements of 67% under far-fault loading and 73% under near-fault loading. Among variable models, SSCSW PL7 showed the most favorable results, with a 49% increase in energy dissipation relative to the base SSCSW.

3. Damage patterns demonstrated that under near-fault loading, the concrete cover experienced rapid crushing, reaching nearly 60% failure in the first cycle and complete failure by the fifth cycle. In contrast, under far-fault loading, concrete degradation was gradual, with full collapse occurring by the tenth cycle.

4. Stress distribution analyses revealed that the highest Von Mises stresses developed in the panel zone and at secondary column-to-beam connections, in some cases leading to element removal when stresses exceeded the ultimate strength of steel.

5. Overall, the results confirm that composite semi-supported walls exhibit superior cyclic and monotonic performance compared to conventional semi-supported walls. However, the sudden

degradation of concrete under near-fault loading emphasizes the need for careful consideration of main frame elements and boundary member design.

Future research should explore more refined numerical models incorporating plate tearing and realistic stud or bolt connections, as well as experimental validation of semi-supported composite walls under different loading protocols. Additionally, the potential link-beam behavior of the beam segment between secondary and primary columns requires detailed nonlinear evaluation.

7- References

[1] Wallace, J. W& . Moehle, J. P., (1992). Ductility and detailing requirements of bearing wall buildings, J. Struct. Eng, 10.1061/ (ASCE), pp. 1625–1644.
DOI:10.1061/(ASCE)0733-9445(1992)118:6(1625)

[2] Rahimi, T. Kheyroddin, A. and Gholhaki, M. 2020. An Analytical and Numerical Study on Effect of Thickness and Concrete Type of Panels on Behavior of Composite Steel Plate Shear Walls, *Amirkabir J. Civil Eng*,*53*,pp3623-3648. http://dx.doi.org/10.22060/ceej.2020.17929.6713

[3] Gholhaki, M. & Pachideh, G. & Javahertarash, A., (2020). Capacity spectrum of SPSW using pushover and energy method withoutneed for calculation of target point, Structures, Volume. 26, pp. 516-523. https://doi.org/10.1016/j.istruc.2020.04.028

[4] Wang, W. & Ren, Y. & Lu, Z. & Song, J. & Han, B. & Zhou, Y., (2019). Experimental study of the hysteretic behaviour of corrugated steel plate shear walls and steel plate reinforced concrete composite shear walls, Journal of Constructional Steel Research, Volume 160, pp 136–152. DOI:10.1016/j.jcsr.2019.05.019

[5] Jahanpour, A. & Moharrami, H., (2015). Evaluation of behavior of the secondary columns in semi-supported steel shear walls, Thin-Walled Structures, Volume 93, pp. 94-101.
https://doi.org/10.1016/j.tws.2015.03.015

[6] Siahpolo, N. & Bahmaie, J., (2021). Evaluation of behavior of semi-supported steel shear walls against monotonic and cyclic loading, Amirkabir J. Civil Eng, Volume 53, pp. 18-33. 10.22060/ceej.2020.17039.6434

[7] Jahanpour,A. & Moharrami, H., 2017. Limit analysis and design of semi-supported steel shear walls, Tarbiat Modares University Tehran publications, https://doi.org/10.1016/j.engstruct.2017.01.004

[8] Aragheizadeh, E. & Tabatabaei Mirhosseini, R., (2021). Effect of Tensile Damage Parameter Reducing in Non-linear Analysis of Reinforced Concrete Structures using Concrete Damage Plasticity Method, Amirkabir J. Civil Eng, Volume 53, pp. 57-70.
10.22060/ceej.2021.19021.7031

[9] Faleiro, J. & Oller, S. & Barbat, A.H., (2010). Plastic-damage analysis of reinforced concrete frames, Engineering Computations, Volume 27, pp. 57-83.
https://doi.org/10.1108/02644401011008522

[10] Hassani Sokhtesaraei, M. Ghassemieh, M. and Mirghaderi, S R. 2019. Comparing Seismic Performance of WUF-W & RBS Moment Connections in Box-Section Columns Under SAC & ATC-24 Loading Protocols, Journal of structure & steel, 13, pp 91-109.

http://dx.doi.org/20.1001.1.1735515.1398.1398.26.1.7 \

[11] Zhao, Q. and Astaneh-Asl, 2004. A.Cyclic behavior of traditional and innovative composite shear walls, Journal Of Structural Engineerrng, 130, pp 271-284. https://doi.org/10.1061/(ASCE)0733-9445(2004)130:2(271)

[12] AISC, "Load and Resistance Factor Design (LRFD) Specification for Structural Steel Buildings is based on reliability theory", USA, Chicago.(1999).

[13] Jahanpour, A. & Moharrami, H. & Jönsson, J., (2012). Seismic behavior of semi-supported steel shear walls, Journal of Constructional Steel Research, Volume 74, pp. 118-133. https://doi.org/10.1016/j.jcsr.2012.02.014

[14] ABAQUS."Standard is a general-purpose, finite element module", Version 20.00, reference manual, ABAQUS Inc.(2020).

[15] AISC 341-22, (2022). supersedes the seismic Provisions for Structural Steel Buildings, USA. Chicago. https://www.aisc.org/globalassets/aisc/publications/standards/a341-22w.pdf

[16] ETABS."Extended Three Dimensional Analysis and Design of Building System", Version 20.00, Computers and structures, Berkeley, CA, USA,(2020).

[17] Jahanpour,A. & Moharrami, H., (2017). Software Design and control of semi-supported steel shear walls. Tarbiat Modares University Tehran publications.

[18] Standard No 2800. 2015. Iranian Code of Practice for Seismic Resistant Design of Buildings, 4th Edition, Building and Housing Research Center, Tehran, Iran.

[19] National Building Regulation No 10. 2022. Design and implementation of steel buildings, Office for Development and Promotion of National Building Regulations, Publications of the Ministry of Housing and Urban Development.

[20] ASCE 7, "Minimum Design Loads and Associated Criteria for Buildings and Other Structures", USA, Virginia.(2022). https://doi.org/10.1061/9780784415788

[21] Hognestad, E,. "A Study of Combined Bending and Axial Load in Reinforced Concrete Members", University of Illinosi Engineering Expriment Station.(2007). https://core.ac.uk/download/pdf/4814295.pdf

[22] Kmiecik, P. & Kaminski, M., (2011). Modelling of reinforced concrete structures and composite structures with concrete strength degradation taken into consideration, Archives Of Civil And Mechanical Engineering , Volume. Xi. pp. 623–636. https://doi.org/10.1016/S1644-9665(12)60105-8Get rights and content

[23] Krawinkler, H. Gupta, A. Medina, R. and Luco, N., "Development of Loading Histories for Testing of Steel Beam to-Column Assemblies", SAC Background Report, SAC/BD-00/10.(2000).

[24] European convention for constructional steelwork., (1986). Recommended testing procedure for assessing the behaviour of structural steel elements under cyclic loads, Brussels. Belgium. ECCS.

Funding

This research received no specific grant from any funding agency in the public, commercial, or not-for-profit sectors.

Data Availability

The data that support the findings of this study are available from the corresponding author upon reasonable request.

Author Contributions

Sina Momeni: Performed the main manuscript writing, numerical modeling, and analysis.

Navid Siahpolo: Reviewed the data and contributed to manuscript revision.

Alireza Jahanpour: Contributed to the validation section of the study.

All authors read and approved the final version of the manuscript.

Conflict of Interest

The authors declare that there is no conflict of interest regarding the publication of this paper.